SHOCK WAVE STRUCTURE IN MIXTURES OF GASES WITH GREATLY DIFFERING MOLECULAR MASSES

G. A. Ruev, V. M. Fomin, and M. Sh. Shavaliev

UDC 533.6.011.8

The flow of mixtures of gases with greatly differing molecular masses under rapid acceleration or braking of the flow with high gradients in hydrodynamic quantities which occurs in shock waves cannot be described within the framework of conventional, i.e., single-velocity, single-temperature Navier–Stokes equations. Because of the high inertia of the heavy molecules in such flows a velocity "slip" develops between the mixture components, and in view of the difficulty of energy exchange between molecules with a large mass difference each component establishes its own temperature. The difference in hydrodynamic velocities of the components which often develops and the temperature difference are comparable to the velocities and temperatures themselves. In these cases one must employ the equations of multivelocity multitemperature mixture gas dynamics (multiliquid hydrodynamic equations) in which each component (or group of components) is characterized by its own hydrodynamic velocity and temperature. The problem of shock wave structure in a mixture of gases with greatly differing molecular masses ($\varepsilon = m_1/m_2 \ll 1$) was solved in [1] using the equations of two-velocity two-temperature gas dynamics [2, 3]. However, the partial viscosity and thermal conductivity coefficients appearing in these equations are equal to the corresponding coefficients of the pure gases. This leads to a situation where calculation results agree with experimental data and calculations based on kinetic equations for only a narrow range of heavy component concentration. It was concluded in [1] that to expand the range of applicability of these equations it would be necessary to use more general expressions for the partial transport coefficients which depend on concentration and the parameters of the other component.

In [4], equations with such coefficients were obtained from a system of 13-moment (for each mixture component) equations [5, 6] and used to solve the problem of structure of a moderate intensity shock wave in He–Ar and He–Xe gas mixtures. Below we will offer a detailed study of this problem, present new results, and analyze the same.

1. Basic System of Equations and Formulation of the Problem. For the one-dimensional case the system of equations of two-velocity two-temperature gas dynamics has the form [4]

$$\frac{\partial \rho_i}{\partial t} + \frac{\partial \rho_i u_i}{\partial x} = 0, \quad i = 1, 2, \ j \neq i,$$

$$\rho_i\left(\frac{\partial u_i}{\partial t} + u_i \frac{\partial u_i}{\partial x}\right) = -\frac{\partial p_i}{\partial x} - F_{ij} + \frac{4}{3}\frac{\partial}{\partial x}\left(\mu_i \frac{\partial u_i}{\partial x}\right),$$

$$\frac{3}{2}\rho_i R_i\left(\frac{\partial T_i}{\partial t} + u_i \frac{\partial T_i}{\partial x}\right) = -p_i \frac{\partial u_i}{\partial x} - Q_{ij} + \beta_i F_{ij} u_{ij} + \frac{\partial}{\partial x}\left(\lambda_i \frac{\partial T_i}{\partial x}\right) + \tag{1.1}$$

$$+ \frac{4}{3}\mu_i\left(\frac{\partial u_i}{\partial x}\right)^2, \quad F_{ij} = K u_{ij}, \quad Q_{ij} = q(T_i - T_j), \quad u_{ij} = u_i - u_j,$$

$$p_i = \rho_i R_i T_i, \quad \beta_i = \frac{T_i}{m_i}\left/\left(\frac{T_1}{m_1} + \frac{T_2}{m_2}\right)\right.$$

Here ρ_i, u_i, and T_i are the mass density, velocity, and temperature of component i; $n_i = \rho_i/m_i$; $R_i = k/m_i$; k is Boltzmann's constant. The coefficients K and q, which characterize exchange of momentum and energy between the mixture components and the partial viscosity μ_i and thermal conductivity λ_i coefficients will be written in the form of [4]

$$K = \frac{16}{3}\frac{\rho_1\rho_2}{m_1 + m_2}\Omega_{12}^{(1,1)}, \quad q = \frac{3k}{m_1 + m_2}K,$$

Novosibirsk. Translated from Zhurnal Prikladnoi Mekhaniki i Tekhnicheskoi Fiziki, No. 4, pp. 26-33, July-August, 1989. Original article submitted November 30, 1987; revision submitted February 17, 1988.

 0021-8944/89/3004-0532$12.50

$$\mu_1 = \frac{5}{8} kT_1 \left(\Omega_1^{(2,2)} + 2 \frac{n_2}{n_1} \Omega_{12}^{(2,2)} \right)^{-1}, \quad \mu_2 = \frac{5}{8} kT_2 \left(\Omega_2^{(2,2)} + \frac{20}{3} \frac{\rho_1}{\rho_2} \Omega_{12}^{(1,1)} \right)^{-1}, \tag{1.2}$$
$$\lambda_1 = \frac{75}{32} \frac{k^2 T_1}{m_1} \left(\Omega_1^{(2,2)} + 5 \frac{n_2}{n_1} \Omega_{12}^{(1,1)} \right)^{-1}, \quad \lambda_2 = \frac{75}{32} \frac{k^2 T_2}{m_2} \left(\Omega_2^{(2,2)} + 15 \frac{\rho_1}{\rho_2} \Omega_{12}^{(1,1)} \right)^{-1}.$$

Equations (1.1) and (1.2) do not include terms which vanish for the case of a Maxwell molecule model, while Q_{ij} and the partial stress tensors also omit terms $\sim u_{ij}^2$ (in view of the condition $u_{ij}/\sqrt{2kT_1/m_1} \ll 1$ [3]). The kinetic coefficients μ_i and λ_i are expanded in ε and terms of order ε are dropped (but terms $\sim \varepsilon n_1/n_2$ are retained for $\rho_1 \gtrsim \rho_2$).

We note that Eq. (1.2) transforms to the expressions of [2] under the assumptions made therein, while Eqs. (1.1) and (1.2) transform into the Navier–Stokes equations when single-velocity single-temperature flow is realized. Therefore, it can be expected that Eq. (1.1) with Eq. (1.2) will describe shock-wave structure over a wide range of concentration values for the heavy component x_2 ($x_i = n_i / (n_1 + n_2)$).

We must find a steady-state solution of system (1.1) satisfying the boundary conditions

$$\begin{aligned} (\rho_i, u_i, T_i) &\to (\rho_i^0, u_i^0, T_i^0), \quad x \to -\infty, \\ (\rho_i, u_i, T_i) &\to (\rho_i^1, u_i^1, T_i^1), \quad x \to +\infty \end{aligned} \tag{1.3}$$

(the subscript 0 denotes parameters of the incident flow, while quantities with the subscript 1 are related to parameters of the incident flow by the Hugoniot relationships for an equilibrium mixture).

To perform calculations it will be convenient to transform to dimensionless variables

$$\begin{gathered} \bar{\rho}_i = \rho_i/\rho_i^0, \quad \bar{u}_i = u_i/\sqrt{R^0 T^0}, \quad \bar{T}_i = T_i/T^0, \quad \bar{p}_i = p_i/(\rho_i^0 R^0 T^0), \\ \bar{R}_i = R_i/R^0, \; R^0 = kn^0/\rho^0, \; \bar{x} = x/L^*, \; \bar{t} = t\sqrt{R^0 T^0}/L^*, \\ L^* = \mu^*/(\rho^0 u^0), \end{gathered} \tag{1.4}$$

where u^0 is the incident flow velocity, μ^* is the gas mixture viscosity coefficient under sonic conditions [i.e., at a temperature $T^* = 3T^0(1 + M_0^2/3)/4$, $M_0 = u^0/a^0$] which is calculated with Wilke's expression [7]. (In the case of solid-sphere molecules the spatial variable is dedimensionalized using the molecular free path length in the incident flow L^-, as defined in [8]). In the variables of Eq. (1.4), Eq. (1.1) and boundary conditions (1.3) have the form

$$\frac{\partial \bar{\rho}_i}{\partial \bar{t}} + \frac{\partial \bar{\rho}_i \bar{u}_i}{\partial \bar{x}} = 0, \quad i = 1, 2, \quad j \neq i,$$
$$\bar{\rho}_i \left(\frac{\partial \bar{u}_i}{\partial \bar{t}} + \bar{u}_i \frac{\partial \bar{u}_i}{\partial \bar{x}} \right) = -\frac{\partial \bar{p}_i}{\partial \bar{x}} - \bar{K}_i \bar{u}_{ij} + \frac{4}{3} \frac{\partial}{\partial \bar{x}} \left(\bar{\mu}_i \frac{\partial \bar{u}_i}{\partial \bar{x}} \right),$$
$$\frac{3}{2} \bar{\rho}_i \bar{R}_i \left(\frac{\partial \bar{T}_i}{\partial \bar{t}} + \bar{u}_i \frac{\partial \bar{T}_i}{\partial \bar{x}} \right) = -\bar{p}_i \frac{\partial \bar{u}_i}{\partial \bar{x}} - \bar{q}_i (\bar{T}_i - \bar{T}_j) + \tag{1.5}$$
$$+ \beta_i \bar{K}_i \bar{u}_{ij}^2 + \frac{\partial}{\partial \bar{x}} \left(\bar{\lambda}_i \frac{\partial \bar{T}_i}{\partial \bar{x}} \right) + \frac{4}{3} \bar{\mu}_i \left(\frac{\partial \bar{u}_i}{\partial \bar{x}} \right)^2;$$
$$\begin{aligned} &\bar{\rho}_i = 1, \; \bar{u}_i = \bar{u}^0 = \sqrt{5/3} M_0, \; \bar{T}_i = 1 && \text{at} \quad \bar{x} = -l, \\ &\bar{u}_i = \bar{u}^1, \; \bar{T}_i = \bar{T}^1 && \text{at} \quad \bar{x} = +l. \end{aligned} \tag{1.6}$$

Here the dimensionless coefficients

$$\bar{K}_i = KL^*/(\rho_i^0 \sqrt{R^0 T^0}), \quad \bar{q}_i = qL^*/(\rho_i^0 R^0 \sqrt{R^0 T^0}),$$
$$\bar{\mu}_i = \mu_i/(\rho_i^0 \sqrt{R^0 T^0} L^*), \quad \bar{\lambda}_i = \lambda_i/(\rho_i^0 R^0 \sqrt{R^0 T^0} L^*)$$

are introduced together with the dimensionless velocity and temperature behind the shock wave

$$\bar{u}^1 = \frac{\sqrt{15}}{4M_0} \left(1 + \frac{M_0^2}{3} \right), \quad \bar{T}^1 = 1 + \frac{1}{5} \left(\frac{5}{3} M_0^2 - (\bar{u}^1)^2 \right).$$

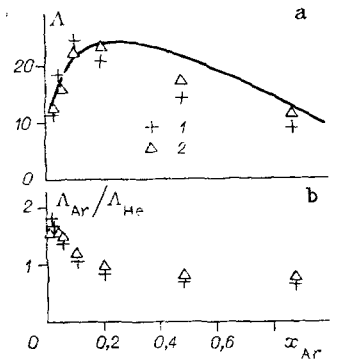

Fig. 1

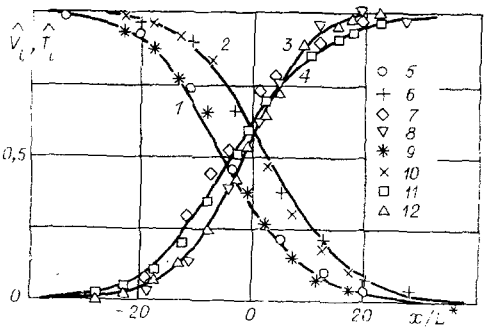

Fig. 2

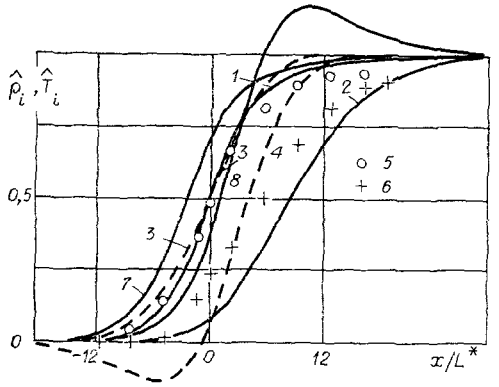

Fig. 3

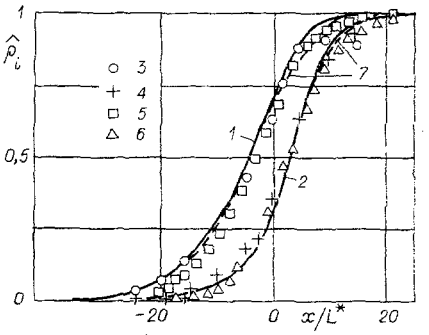

Fig. 4

The value of ℓ is chosen on the basis of numerical experiments such that expansion of the integration region does not lead to change in the computation results.

To model the kinetic coefficients of Eq. (1.2) we express the Ω-integrals appearing therein in terms of the viscosity and thermal conductivity coefficients $[\mu_i]_1$ and $[\lambda_i]_1$ of the pure gas of type i and the diffusion coefficient for the mixture $[D_{ij}]_1$ using expressions obtained in the first approximation in Sonin polynomials [9]. We then assume that the intermolecular interaction potentials are expressible in powers and write $[\mu_i]_1$, $[\lambda_i]_1$, and $[D_{ij}]_1$ in terms of their values in the incident flow. As a result we have

$$K = \frac{kT^0}{m_1 m_2 n^0 [D_{12}^0]_1}\left(\overline{T}_2 + \frac{1}{\varepsilon}\overline{T}_1\right)^{\nu_{12}}, \quad q = \frac{3k}{m_1 + m_2}K,$$

$$\mu_1 = [\mu_1]_1\left(1 + \frac{3}{5}\frac{n_2}{n_1}\frac{AK[\mu_1]_1}{\varepsilon p_1\rho_2}\right)^{-1}, \quad \mu_2 = [\mu_2]_1\left(1 + \frac{6K[\mu_2]_1}{p_2\rho_2}\right)^{-1},$$

$$\lambda_1 = [\lambda_1]_1\left(1 + \frac{3}{2}\frac{n_2}{n_1}\frac{K[\mu_1]_1}{\varepsilon p_1\rho_2}\right)^{-1}, \quad \lambda_2 = [\lambda_2]_1\left(1 + \frac{9}{2}\frac{K[\mu_2]_1}{p_2\rho_2}\right)^{-1},$$

$$[\mu_i]_1 = [\mu_i^0]_1\overline{T}_i^{\nu_i}, \quad [\lambda_i]_1 = \frac{5}{2}\frac{k}{\mathrm{Pr}_i m_i}[\mu_i]_1, \quad A = \Omega_{12}^{(2,2)}/\Omega_{12}^{(1,1)},$$

where Pr_i is the Prandtl number of gas i. The exponents ν_i and ν_{12} were selected using experimental data on the viscosity of gas i and diffusion in the mixture, respectively [7, 9, 10]:

$$\nu_1(\mathrm{He}) = 0.647, \ \nu_2(\mathrm{Ar}) = 0.816, \ \nu_2(\mathrm{Xe}) = 0.93,$$
$$\nu_{12}(\mathrm{He} - \mathrm{Ar}) = 0.25, \ \nu_{12}(\mathrm{He} - \mathrm{Xe}) = 0.32.$$

For proper comparison with results obtained by the Monte Carlo direct statistical modeling method, calculations were performed for a model of the molecules as elastic solid spheres ($\nu_i = \nu_{12} = 0.5$) with effective molecular diameter ratios [8] $\sigma_{He}/\sigma_{Ar} = 2.19/3.66$, $\sigma_{He}/\sigma_{Xe} = 2.19/4.94$.

To solve the problem of Eqs. (1.5) and (1.6) we use the determination method, i.e., we seek a solution of the nonsteady-state equations in a coordinate system moving with the wave, with subsequent exit to a steady-state regime. To approximate Eq. (1.5) an implicit difference method involving splitting of the physical processes was used, the method being described in detail in [1].

2. Calculation Results and Evaluation. A series of calculations was performed for an incident flow Mach number range $M_0 = 1.58$-4, while at each value of M_0 calculations were performed for three values of the heavy component concentration, in the ranges of low (1.5-5%), moderate (10-15%), and large (≈50%) concentrations.

The simplest parameter characterizing shock-wave structure is the "effective thickness" of the shock wave, as defined by the maximum slope of the mixture mass density profile $\Lambda = (\hat{\rho}^1 - \hat{\rho}^0)/(d\hat{\rho}/d\bar{x})_{max}$ (Prandtl formula). We also introduce an "effective thickness" for the shock wave in each mixture component, defined by the maximum slope of the partial density $\Lambda_i = (\hat{\rho}_i{}^1 - \hat{\rho}_i{}^0)/(d\hat{\rho}_i/d\bar{x})_{max}$.

Figure 1a, b shows calculated and experimental results for Λ and $\Lambda_{Ar}/\Lambda_{He}$ at $M_0 \approx 2$ and various Ar concentrations (1, calculation; 2, experiment [11]). It is evident that the calculations describe the experimental data satisfactorily over the entire concentration range. Also shown is the analytical solution for thickness of a weak shock wave [4] (line). It is evident that this solution, although obtained as $M_0 \to 1$, can be used to determine shock-wave thickness for M_0 values up to two. We note that from some value $x_{Ar}\Lambda_{Ar} < \Lambda_{He}$. However, the graphs of partial densities ρ_i in the shock wave presented below show that the width of the transition layer [defined by Taylor as the distance between points at which $(\rho_i - \rho_i{}^0)/(\rho_i{}^1 - \rho_i{}^0) = 0.05$ and $(\rho_i{}^1 - \rho_i)/(\rho_i{}^1 - \rho_i{}^0) = 0.05$] for the heavy component is always larger than that of the light component. This contradiction indicates the limited applicability of the Prandtl expression for determination of shock-wave thickness in mixtures.

Figures 2-5 show profiles of partial densities, velocities, and temperatures in the shock wave, defined in the form $\hat{V}_i = (\bar{u}_i - \bar{u}^1)/(\bar{u}^0 - \bar{u}^1)$, $\hat{T}_i = (\bar{T}_i - 1)/(\bar{T}^1 - 1)$, $\hat{\rho}_i = (\bar{\rho}_i - 1)/(\bar{\rho}_i{}^1 - 1)$ $(\bar{\rho}_i{}^1 = \bar{u}^0/\bar{u}^1)$. The origin is taken at the point where the numerical density of the mixture has changed to half of its change in the shock wave, i.e., $x_1{}^0\hat{\rho}_1 + x_2{}^0\hat{\rho}_2 = 0.5$ at $x = 0$. The results of the present study are shown by solid lines. Results of calculations in an He–Ar mixture are also compared with experimental data and numerical modeling with kinetic equations.

Initially calculations were performed for $M_0 < 2$ and moderate Ar concentrations ($M_0 = 1.58$, 11% Ar in Fig. 2), while there is no doubt that the equations of a continuous medium are operative. The convincing agreement with experimental [12] and calculated [13] data is evident (1, 5, 9, $\hat{V}_{He}$; 2, 6, 10, $\hat{V}_{Ar}$; 3, 7, 11, $\hat{T}_{He}$; 4, 8, 12, $\hat{T}_{Ar}$; 5-8, experiments of [12]; 9-12, calculation by the Monte Carlo method for the BCH model [13]). The effects of "separation of the mixture components over velocity and temperature begin to appear from $M_0 \approx 2$, especially at low concentrations of the heavy gas (Fig. 3, $M_0 = 2.07$, 2.2% Ar: 1, 3, 5, $\hat{\rho}_{He}$; 2, 4, 6, $\hat{\rho}_{Ar}$; 3, 4, calculation by Navier–Stokes equations [14]; 5, 6, experiments of [11], 7, $\hat{T}_{He}$; 8, $\hat{T}_{Ar}$). The solution of the Navier–Stokes equations leads to a nonmonotonic heavy component density profile [14]. As has been noted in the literature, such a profile, which according to the relationship $\rho_i u_i = C_i = \text{const}$ indicates acceleration of the heavy gas in the initial portion of the shock wave and subsequent braking, has no physical meaning and contradicts the experimental data [11]. The solution using the model of Eqs. (1.1) and (1.2) agrees with experiment.

For Mach numbers close to two, calculations with moderate (13%) and large (48%) argon concentrations lead to more complete agreement with experiments. Moreover, at 48% Ar, where conditions are realized for single-temperature single-velocity description of the mixture, Eqs. (1.1) and (1.2) and the Navier–Stokes equations yield coinciding results over almost the entire shock-wave width (Fig. 4, $M_0 = 2.24$: 1, 3, 5, $\hat{\rho}_{He}$; 2, 4, 6, $\hat{\rho}_{Ar}$; 3-6, experiments of [11, 15]; 7, calculation, Navier–Stokes equations [14]).

We note that even at $M_0 = 3$ there is good agreement with the results of numerical solution of the BCH model of the Boltzmann equation [16] (Fig. 5, 10% Ar: 1, 5, $\hat{V}_{He}$; 2, 6, $\hat{V}_{Ar}$; 3, 7, $\hat{T}_{He}$; 4, 8, $\hat{T}_{Ar}$; 5-8, BCH model).

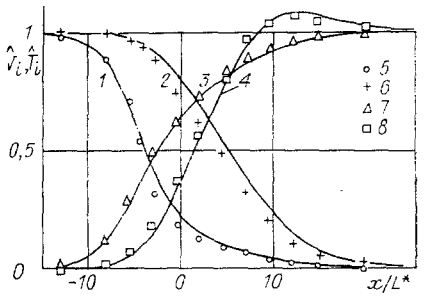

Fig. 5

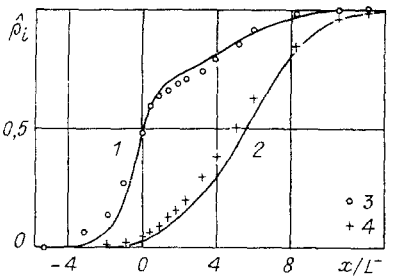

Fig. 6

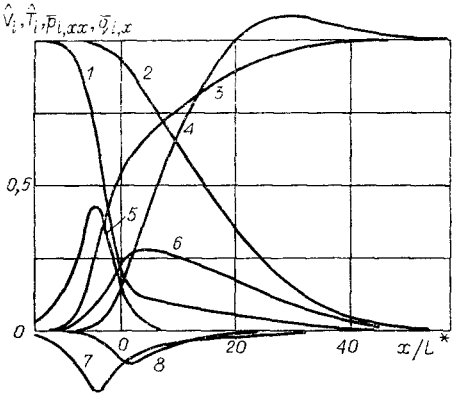

Fig. 7

Similar calculations were performed for an He–Xe mixture, where one could expect that the effects caused by the difference in molecular masses ($\varepsilon \approx 3 \cdot 10^{-2}$) would appear still more strongly. Results for the case $M_0 = 3.89$ and 3% Xe are shown in Figs. 6 and 7. The density data are sufficiently close to those obtained by the Monte Carlo method [17] (Fig. 6: 1, 3, $\hat{\rho}_{He}$; 2, 4, $\hat{\rho}_{Ar}$; 3, 4, [17]). Figure 7 shows profiles of partial velocities and temperatures (1, $\hat{V}_{He}$; 2, $\hat{V}_{Xe}$; 3, $\hat{T}_{He}$; 4, $\hat{T}_{Xe}$).

The results presented permit establishment of some features of shock-wave structure in mixtures of gases with a large difference between molecular masses. It is evident from the graphs that within the shock wave large differences develop between the velocities and temperatures of the mixture components [$(u_2 - u_1) \sim u_i$, $|T_1 - T_2| \sim T_i$], which justifies the use of two-speed two-velocity equations.

By numerical modeling of the kinetic equations the authors of [16, 18] observed a nonmonotonic temperature profile for the heavy-mixture component at small concentration levels. The heavy gas temperature increases to some value exceeding the equilibrium temperature behind the shock wave and thereafter decreases, tending to that value. The present calculations also confirm the presence of this nonmonotonicity. In particular, comparison with the results of [16] indicates agreement in the value and position of the temperature peak (see Fig. 5). With the aid of detailed calculations the dependence of the temperature peak on concentration, M_0, and the molecular mass ratio ε was established. This dependence decreases with increase in heavy gas concentration ahead of the shock wave and increases with growth in M_0 for a fixed concentration. It follows from comparison of the results for He–Ar and He–Xe that with decrease in ε for a fixed value of heavy gas concentration x_2 the temperature peak decreases. Its maximum value is shifted toward lower gas concentrations. For a fixed mass concentration the maximum value of the heavy-component concentration increases with increase in both M_0 and m_2/m_1, which agrees qualitatively with [19].

We will offer some comments to clarify the mechanism of temperature peak formation. In a steady-state shock wave the velocity of the heavy component (in view of the higher inertia of its molecules) always exceeds the velocity of the lighter component. More abrupt braking of the lighter component leads, on the one hand, to an increase in its temperature, which in the initial segment of the shock wave is always higher than the heavy gas temperature and, on the other, to enrichment of the mixture by the light gas. As a result of this enrichment energy supply to the heavy gas increases due to operation of the intercomponent

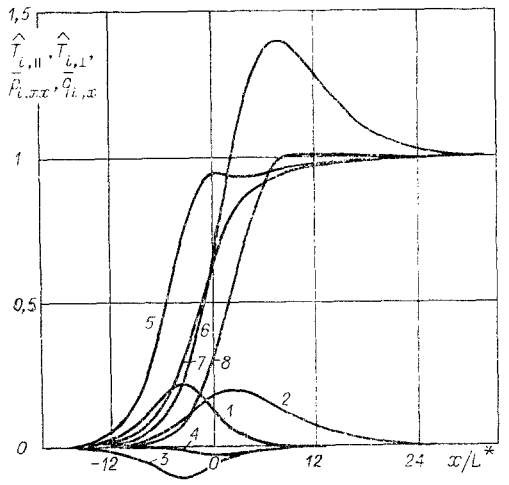

Fig. 8

interaction force F_{ij}. In fact, as follows from the energy equations of Eq. (1.1), such energy supply is equal to $\beta_2 F_{12} u_{12}/n_2$ per molecule in the heavy gas and $\beta_1 F_{12} u_{12}/n_1$ in the light one. Their ratio is $\beta_2 n_1/\beta_1 n_2 \sim m_1 n_1/m_2 n_2 = \rho_1/\rho_2$. If the heavy gas concentration ahead of the wave is low, so that $\rho_2^0 \leq \rho_1^0$, then within the wave $\rho_1/\rho_2 = \rho_1^0 u_2/\rho_2^0 u_1 \gg 1$. Moreover, for sufficient penetration into the shock layer, where $|\nabla u_2| \gg |\nabla u_1|$, energy dissipation due to viscosity occurs essentially in the heavy gas. As a result of these factors, as well as heat exchange caused by the temperature difference, intense increase in the temperature of the heavy gas commences. This may lead to the temperature exceeding the equilibrium temperature behind the shock wave. The basic contribution to formation of the temperature peak is produced by the work of the intercomponent interaction force. As was shown in [20], this peak is maintained as the viscosity coefficient tends to zero.

Another characteristic feature of shock-wave structure at low concentration of the heavy component is a clearly expressed shock transition zone, in which the parameters of the light component change abruptly, while those of the heavy gas are practically constant, and a relaxation zone, in which the mixture enters an equilibrium state behind the shock wave (see Figs. 6 and 7).

Figures 7 and 8 show graphs of the ratios of the viscous stress tensor $p_{i,xx}$ to the pressure and of the thermal flux $q_{i,x}$ to the concrete heat flux in each component of the mixture: $\bar{p}_{i,xx} = p_{i,xx}/p_i$, $\bar{q}_{i,x} = q_{i,x}/(\rho_i c_{pi} T_i u_i)$ $(c_{pi} = 5R_i/2)$. On the one hand these relationships provide certain information on the behavior of $p_{i,xx}$ and $q_{i,x}$ in the shock wave, while on the other they permit determination of the range of applicability of Eqs. (1.1) and (1.2) with respect to Mach number. In reality, $\bar{p}_{i,xx}$ and $\bar{q}_{i,x}$ are the ratios of the Navier–Stokes corrections in the stress tensor and thermal flux to the corresponding Euler terms and, therefore, should remain small quantities of the order of magnitude of the Knudsen number. In the He–Ar mixture they do not exceed 0.2 at $M_0 = 2.07$ (Fig. 8, with 2.2% Ar: 1, $p_{He,xx}$; 2, $p_{Ar,xx}$; 3, $q_{He,x}$; 4, $q_{Ar,x}$), but reach values of 0.63 at $M_0 = 4$, while in the He–Xe mixture at $M_0 = 3.89$ they reach 0.4 (see Fig. 7, where 5, $p_{He,xx}$; 6, $p_{Xe,xx}$; 7, $q_{He,x}$; 8, $q_{Xe,x}$). These data indicate that in an He–Ar mixture at $M_0 = 4$ the equations are clearly inapplicable, while in an He–Xe mixture $M_0 = 3.5$ is the upper limit.

Of interest is the question of partial temperature anisotropy $(T_{i,\parallel} - T_{i,\perp})/T_i$ in the shock wave, where the longitudinal and perpendicular temperature components are defined by the expressions

$$\bar{T}_{i,\parallel} = T_{i,\parallel}/T_i = 1 + \bar{p}_{i,xx}, \quad \bar{T}_{i,\perp} = T_{i,\perp}/T_i = 1 - \bar{p}_{i,xx}/2.$$

(Such a definition of $T_{i,\parallel}$ and $T_{i,\perp}$ is not precise, but provides a qualitative description and permits approximate determination of the conditions under which they must be introduced. In a precise approach one would introduce longitudinal and transverse temperatures as early as the asymptotic solution of Boltzmann's equation and the derivation of the gas dynamic equations.) Hence, the anisotropy is equal to $(\bar{T}_{i,\parallel} - \bar{T}_{i,\perp}) = 3\bar{p}_{i,xx}/2$ and is small within the range of applicability of the initial equations. Figure 8 shows graphs of $\hat{T}_{i,\parallel}$ and $\hat{T}_{i,\perp}$ (5, $\hat{T}_{He,\parallel}$; 6, $\hat{T}_{Ar,\parallel}$; 7, $\hat{T}_{He,\perp}$; 8, $\hat{T}_{Ar,\perp}$). Here the large difference of longitudinal

temperatures from transverse is caused by the choice of $\hat{T}_{i,\parallel(\perp)}$ in place of $\bar{T}_{i,\parallel(\perp)}$. A temperature peak appears in the longitudinal temperature component of the heavy-mixture component.

It follows from the calculations performed and comparison of the results with available experimental data and calculations using the kinetic equations that the equations of two-velocity two-temperature gas dynamics, Eqs. (1.1) and (1.2) are applicable for describing shock wave structure in gas mixtures at Mach numbers up to 3.5 over a wide range of heavy-mixture component concentrations (from 1 to 50%).

LITERATURE CITED

1. G. A. Ruev, V. M. Fomin, and M. Sh. Shavaliev, "Shock-wave structure in a two-velocity two-temperature mixture of viscous thermally conductive gases," ChMMSS, 17, No. 2 (1986).
2. V. V. Struminskii, "Effect of diffusion velocity on gas mixture flow," Prikl. Mat. Mekh., 38, No. 2 (1974).
3. V. V. Struminskii and M. Sh. Shavliev, "Transport phenomena in multivelocity and multitemperature gas mixtures," Prikl. Mat. Mekh., 50, No. 1 (1986).
4. G. A. Ruev, V. M. Fomin, and M. Sh. Shavaliev, "Sound propagation and shock-wave structure in two-velocity and two-temperature gas mixtures," in: Numerical and Analytical Methods in Rarefied Gas Dynamics: Proceedings of the 8th All-Union Conference on Rarefied Gas Dynamics, Mosk. Aviats. Inst., Moscow (1986).
5. V. I. Kurochkin and B. M. Markeev, "On transport equations for a multicomponent gas mixture," Zh. Tekh. Fiz., 49, No. 8 (1979).
6. V. Yu. Velikodnyi, "Equations of motion of a gas mixture at finite Knudsen numbers," in: Proceedings of the 6th Young Scholars Conference, Moscow (1981); Dep. VINITI, July 2, 1981, No. 3278-81
7. J. Hirschfelder, W. Curtiss, and R. Bird, Molecular Theory of Gases and Liquids, Wiley, New York (1964).
8. G. Bird, Molecular Gas Dynamics [Russian translation], Mir, Moscow (1981).
9. S. Chapman and T. G. Cowling, Mathematical Theory of Nonuniform Gases, Cambridge Univ. Press, New York (1970).
10. J. Kestin, H. E. Khalita, and W. A. Wakeham, "The viscosity and diffusion coefficients of the binary mixtures of xenon with other noble gases," Physica, 90A, No. 2 (1978).
11. R. E. Center, "Measurement of shock-wave structure in helium–argon mixtures," Phys. Fluids, 10, No. 8 (1967).
12. L. N. Harnett and E. P. Muntz, "Experimental investigation of normal shock-wave velocity distribution functions in mixtures of argon and helium," Phys. Fluids, 15, No. 4 (1972).
13. Yu. N. Grigor'ev and M. S. Ivanov, "The Monte Carlo method and shock-wave structure for binary gas mixtures," ChMMSS, 8, No. 6 (1977).
14. F. S. Sherman, "Shock-wave structure in binary mixtures of chemically inert perfect gases," J. Fluid Mech., 8, Pt. 3 (1960).
15. A. A. Bochkarev, A. K. Rebrov, and N. I. Timoshenko, "Shock wave structure in an Ar–He mixture," Izv. Sib. Otd. Akad. Nauk SSSR, Ser. Tekh. Nauk, No. 3, Issue 1 (1976).
16. K. Abe and H. Oguchi, "Shock-wave structure in binary gas mixtures," in: Rarefied Gas Dynamics, Vol. 1, Academic Press, New York (1969).
17. B. Schmidt, F. Seiler, and M. Worner, "Shock structure near a wall in pure inert gas and in binary inert gas mixtures," J. Fluid Mech., 143, 305 (1984).
18. G. A. Bird, "The structure of normal shock waves in a binary gas mixture," J. Fluid Mech., 31, No. 4 (1968).
19. G. A. Bird, "Shock wave structure in gas mixtures," in: Rarefied Gas Dynamics, Vol. 1, Univ. Tokyo Press (1984).
20. G. A. Ruev and V. M. Fomin, "Shock wave structure in a binary mixture of viscous gases," Zh. Prikl. Mekh. Tekh. Fiz., No. 5 (1984).